Published in final edited form as:
J Comp Neurol. 2009 June 1; 514(4): 353–367. doi:10.1002/cne.22006.

Postnatal Development of Synaptic Structure Proteins in Pyramidal Neuron Axon Initial Segments in Monkey Prefrontal Cortex

Dianne A. Cruz[1,*], **Emily M. Lovallo**[2], **Steven Stockton**[2], **Matthew Rasband**[3], and **David A. Lewis**[1,2]

[1]Department of Psychiatry, University of Pittsburgh, Pittsburgh, PA

[2]Department of Neuroscience University of Pittsburgh, Pittsburgh, PA

[3]Department of Neuroscience Baylor College of Medicine, Houston, TX

Abstract

In the primate prefrontal cortex (PFC), the functional maturation of the synaptic connections of certain classes of GABA neurons is very complex. For example, the levels of both pre- and post-synaptic proteins that regulate GABA neurotransmission from the chandelier class of cortical interneurons to the axon initial segment (AIS) of pyramidal neurons undergo marked changes during both the perinatal period and adolescence in the monkey PFC. In order to understand the potential molecular mechanisms associated with these developmental refinements, we quantified the relative densities, laminar distributions, and lengths of pyramidal neuron AIS immunoreactive for ankyrin-G, ßIV spectrin, or gephyrin, three proteins involved in regulating synapse structure and receptor localization, in the PFC of rhesus monkeys ranging in age from birth through adulthood. Ankyrin-G- and ßIV spectrin-labeled AIS declined in density and length during the first six months postnatal, but then remained stable through adolescence and into adulthood. In contrast, the density of gephyrin-labeled AIS was stable until approximately 15 months of age and then markedly declined during adolescence. Thus, molecular determinants of the structural features that define GABA inputs to pyramidal neuron AIS in monkey PFC undergo distinct developmental trajectories with different types of changes occurring during the perinatal period and adolescence. In concert with previous data, these findings reveal a two-phase developmental process of GABAergic synaptic stability and GABA neurotransmission at chandelier cell inputs to pyramidal neurons that likely contributes to the protracted maturation of behaviors mediated by primate PFC circuitry.

Keywords

ankyrin-G; ßIV spectrin; chandelier cell; $GABA_A$ receptor; gephyrin; working memory

Correspondence: David A. Lewis, MD Department of Psychiatry University of Pittsburgh 3811 O'Hara Street, W1651 BST Pittsburgh, PA 15213 Phone: (412) 624 3934 Fax: (412) 624 9910 E-mail: lewisda@upmc.edu.
*Current affiliation: Department of Psychiatry, University of Texas Health Science Center at San Antonio

Disclosure of Interest David A. Lewis currently receives research support from the BMS Foundation, Bristol-Myers Squibb, Curridium Ltd and Pfizer and in 2006-2008 served as a consultant to AstraZeneca, Bristol-Myers Squibb, Hoffman-Roche, Lilly, Merck, Neurogen, Pfizer, Sepracor and Wyeth. All other authors have no conflicts of interest to disclose.

Introduction

The primate cerebral cortex contains diverse subpopulations of GABA-containing interneurons which differ in their morphological, physiological, and molecular attributes (Ascoli et al., 2008). The resulting specialized functions enable each subpopulation to differentially regulate the activity of excitatory pyramidal neurons (Markram et al., 2004; McBain and Fisahn, 2001). For example, the axon terminals of chandelier (axo-axonic) neurons form distinctive vertical arrays (termed cartridges) that synapse on the axon initial segment (AIS) of pyramidal neurons (Somogyi, 1977), near the site of axon potential generation. A single chandelier cell may innervate over 200 pyramidal neurons (Somogyi et al., 1982), enabling them to contribute to the synchronization of activity in local networks of pyramidal neurons (Klausberger et al., 2003). In addition, due to site-specific regulation of Cl^- ion transport in pyramidal neurons, GABA inputs from chandelier cartridges can, under certain conditions, produce pyramidal neuron depolarization sufficient to fire an action potential (Szabadics et al., 2006; Khirug et al., 2008).

In the monkey prefrontal cortex (PFC), the density of symmetric, presumably GABA, synapses rises rapidly during the third trimester of gestation and perinatal period until stable, adult levels are achieved at three months postnatal (Bourgeois et al., 1994). In contrast, pre- and post-synaptic markers of the functional properties of chandelier axon inputs to the AIS of pyramidal neurons exhibit a very protracted maturation. Pre-synaptically, immunoreactivities for the calcium-binding protein parvalbumin (PV) and the GABA membrane transporter (GAT1) in chandelier axon cartridges are not detectable or low at birth, rise (albeit with different developmental time courses) to peak levels early in postnatal development that are sustained until ~15 months of age, and then rapidly decline during adolescence until stable adult levels are achieved (Anderson et al., 1995; Condé et al., 1996; Cruz et al., 2003). Since chandelier cartridges in the monkey PFC are readily visualized with Golgi staining across postnatal development (Lund and Lewis, 1993), these changes in PV and GAT1 immunoreactivity are likely to reflect shifts in the concentration of these proteins rather than changes in the presence of, or in the density of axon terminals within, chandelier axon cartridges (Cruz et al., 2003). Post-synaptically, $GABA_A$ receptors containing α2 subunits predominate in pyramidal neuron AIS especially in cortical layers 2-4 (Loup et al., 1998). The density of pyramidal neuron AIS immunoreactive for α_2 subunits is high at birth, then significantly declines during adolescence before achieving stable adult levels (Cruz et al., 2003). These findings indicate that both preand postsynaptic markers of GABA neurotransmission undergo significant changes during postnatal development, suggesting that the capacity to synchronize pyramidal neuron output in the PFC might be in substantial flux until adulthood. Interestingly, the time course of these changes parallels the maturation of performance on cognitive tasks (Luna et al., 2004; Crone et al., 2006), such as working memory, that are dependent on GABA neurotransmission in the dorsolateral PFC (Rao et al., 1999; Rao et al., 2000; Sawaguchi et al., 1989).

However, understanding the nature and functional significance of these changes requires knowledge of the developmental changes in other processes that affect GABA neurotransmission at pyramidal neuron AIS. Of particular interest is how GABA synapses are stabilized at the AIS while the functional properties of GABA neurotransmission at this location are changing during postnatal development. The localization to pyramidal neuron AIS of proteins that regulate synapse structure and receptor clustering provides a means to address this question. For example, the 480- and 270-kDa isoforms of ankyrin-G, members of a class of adaptor molecules that link various membrane proteins to the cytoskeleton, are localized to AIS and nodes of Ranvier, including cortical pyramidal neurons (Kordeli et al., 1995). Interestingly, interactions between ankyrin-G and the cell adhesion molecule, neurofascin, are required for the formation and stabilization of GABA synapses at the AIS

of cerebellar Purkinje neurons (Ango et al., 2004). In addition, ßIV spectrin, which is localized to the AIS of pyramidal neurons through its direct interaction with ankryin-G (Yang et al., 2007), is a critical component in the organization and stabilization of membrane proteins at the AIS (Berghs et al., 2000; Lacas-Gervais et al., 2004; Yang et al., 2004). Thus, ankyrin-G and ßIV spectrin, by contributing to the formation and stabilization of membrane protein microdomains (Bennett and Baines, 2001), may play a role in localizing and stabilizing the terminals of chandelier axons to the AIS of pyramidal neurons during development.

In conjunction with the formation of symmetric synapses at pyramidal neuron AIS, the aggregation of $GABA_A$ receptors containing α_2 subunits at this site may be regulated during development by the scaffolding protein gephyrin (Levi et al., 2004; Jacob et al., 2005; Fritschy et al., 2008). Gephyrin forms clusters only in the presence of $GABA_A$ receptors, and facilitates the preferential accumulation of gephyrin-$GABA_A$ receptor clusters postsynaptic to inhibitory terminals (Studler et al., 2005). The experimental removal of gephyrin reduces $GABA_A$ receptor clustering (Yu et al., 2007), and of particular relevance, the clustering of α_2-containing $GABA_A$ receptors is facilitated by the direct binding of α_2 subunits and gephyrin (Tretter et al., 2008). Finally, the indirect interaction of gephyrin with the cell adhesion molecule neurofascin appears to be important in the targeting of GABA terminals to pyramidal neuron AIS (Burkarth et al., 2007). Thus, changes in gephyrin in pyramidal neuron AIS are likely to reflect the development of GABA synapses at this site.

Consequently, in order to understand the contribution of ankyrin-G, ßIV spectrin, and gephyrin to the maturation of chandelier axon inputs, we examined the densities, laminar distribution, and length of pyramidal neuron AIS immunoreactive for these proteins in the PFC from rhesus monkeys ranging in age from birth to adulthood.

Materials and Methods

Animals

Thirty-three rhesus macaque monkeys (*Macaca mulatta*), ranging in age from 2 days to 18 years, were used in this study (Table 1). Animals were divided into 7 age groups as previously described (Erickson and Lewis, 2002). Housing and experimental procedures were conducted in accordance with USDA and NIH guidelines and with the approval of the University of Pittsburgh's Institutional Animal Care and Use Committee. The acquisition of these animals has been previously described (Erickson and Lewis, 2002). Animals less than 6 months of age were housed with their mothers; juveniles 6-24 months were housed in groups, and animals older than 24 months were housed either in pairs, or in single cages, in the same social setting. All animals were experimentally naive at the time of perfusion.

Tissue preparation and immunocytochemistry

Monkeys were anesthetized with ketamine (25 mg/kg) and pentobarbital (30 mg/kg), and then perfused transcardially with 1% paraformaldehyde in phosphate buffer (pH 7.4) at 4°C followed by 4% paraformaldehyde in phosphate buffer, as previously described (Oeth and Lewis, 1993). The brain was immediately removed, cut into blocks, and immersed in buffered 4% paraformaldehyde. Tissue blocks were immersed in increasing gradients of sucrose solutions and stored in a cryoprotectant solution at -30°C (Cruz et al., 2003). We have previously shown that tissue storage under these conditions for extended periods of time does not affect immunoreactivity for a number of proteins (Erickson et al., 1998; Pierri et al., 1999; Cruz et al., 2003). Tissue blocks containing the left PFC were sectioned coronally at 40 μm and every 10^{th} section was stained for Nissl substance with thionin.

These sections were used to identify the location of PFC area 46 on the dorsal bank of the principal sulcus according to cytoarchitectonic criteria (Walker, 1940).

Floating tissue sections containing area 46 were processed with each of the following three antibodies: 1) A monoclonal mouse IgG antibody (1:200 dilution) raised against an epitope in the spectrin-binding domain (amino acids 893-1474) of the 480 kDa and 270 kDa isoforms of ankyrin-G (clone 4G3F8; catalog # sc-12719; Santa Cruz Biotechnology, Inc, Santa Cruz, CA) was demonstrated to be specific by the absence of immunoreactivity in sections from ankyrin-G knock-out mice (Jenkins et al., 2001; Jenkins and Bennett, 2001; Zhou et al., 1998). 2) A polyclonal rabbit IgG antibody (1:750 dilution) raised against the amino acid sequence 2237-2256 corresponding to the specific domain (SD) of βIV spectrin (Berghs et al., 2000) was demonstrated to be specific by the absence of immunoreactivity in the cerebral cortex of mice with a point mutation in the SD region of βIV spectrin [clone C9831-3c provided by Dr. Matthew Rasband (Yang et al., 2004)]. 3) A polyclonal goat anti-gephyrin antibody (1:200 dilution) directed against the C-terminus of the protein (amino acids 710-760; clone R-20; catalog # sc-6411; Santa Cruz Biotechnology, Inc, Santa Cruz, CA) labeled a single band of the appropriate molecular weight in Western blots of mouse and rat brain tissue as reported by the vendor. Additionally, preadsorption of the antibody with an excess of gephyrin peptide prior to exposure to the tissue abolished specific immunoreactivity (data not shown).

Sections processed for ankyrin-G were incubated for 1 hour in a blocking solution of 0.3% Triton-X 100, 5% normal donkey serum (NDS), 1% bovine serum albumin (BSA), 0.1% lysine, and 0.1% glycine in 0.1M phosphate buffered saline (PBS; pH 7.4), followed by incubation in the blocking solution containing the primary antibody for 48 hours at 4°C. Sections were rinsed in 0.1M PBS followed by a 1 hour incubation in a biotinylated donkey anti-mouse secondary antibody (1:250; Vector Laboratories, Burlingame, CA) in the blocking solution. Sections were processed using the avidin-biotin peroxidase method (Hsu et al., 1981; Vector Laboratories, Burlingame, CA) and immunoreactivity for ankyrin-G was visualized with a diaminobenzidine reaction product followed by osmium tetroxide stabilization (Lewis et al., 1986) and silver nitrate and gold chloride intensification (Pucak et al., 1996).

Antigen retrieval methods were used to visualize βIV spectrin-SD and gephyrin immunoreactivity (Jiao et al., 1999). Tissue sections were immersed in a 0.01M sodium citrate solution (pH 8.5) at 80°C in a water bath for 75 minutes, cooled to room temperature, rinsed in 0.1M phosphate buffer (pH 7.4), and incubated in 1% $NaBH_4$ for 30 minutes. After several rinses over 30 minutes, sections were pretreated in a blocking solution containing 0.3% Triton-X 100, 4.5% normal donkey serum, and 4.5% normal human serum in .05M PBS, followed by incubation in the primary antibody prepared in a blocking solution containing 0.3% Triton-X 100, 3% NDS, 3% normal human serum, and .05% BSA in 0.1M PBS for 48 hours at 4°C. Sections were rinsed in 0.1M PBS (pH 7.4) and incubated in biotinylated donkey anti-rabbit secondary antibody (1:200; Vector Laboratories, Burlingame, CA) for 1 hour. Sections were processed using the avidin-biotin peroxidase method ((Hsu et al., 1981); Vector Laboratories, Burlingame, CA) and immunoreactivity for βIV spectrin-SD was visualized with a diaminobenzidine reaction product followed by osmium tetroxide stabilization (Lewis et al., 1986) and silver nitrate and gold chloride intensification (Pucak et al., 1996).

Two sets of three adjacent sections per subject, with each set separated by approximately 400 μm, were used in these studies. Within each set, one section was processed for ankyrin-G, βIV spectrin-SD, and gephyrin immunoreactivity. For each antibody, one section from each monkey was processed together in the same immunocytochemistry run.

Quantification of labeled cartridges and AIS

We first determined the relative densities of ankyrin-G-, βIV spectrin-SD-, and gephyrin-immunoreactive (IR) AIS across all cortical layers in PFC area 46. For each section, a contour was drawn around the portion of the dorsal bank of the principal sulcus that was cut perpendicular to the pial surface. Using the Stereo Investigator fractionator program (MicroBrightfield, Inc., Colchester, VT), a sampling grid was randomly placed over the contour. A counting frame within each grid square defined the area to be quantified. The sampling grid and counting frame sizes, respectively, were as follows: for ankyrin-G-IR AIS, 450 μm × 450 μm and 75 μm × 75 μm; for βIV spectrin-SD-IR AIS, 450 μm × 450 μm and 65 μm × 65 μm; and for gephyrin-IR AIS, 300 μm × 300 μm and 100 μm × 100 μm. Labeled AIS were identified according to previously published criteria (Cruz et al., 2003) as distinct, intensely immunoreactive vertical structures, located immediately below the cell body of unlabeled pyramidal neurons and tapering in diameter in the direction from the pial surface to the white matter (Fig. 1). Using a 40x PlanApo objective, all AIS that met criteria and fell within the inclusion boundaries of a counting frame were identified on a monitor at a final magnification of 960x.

A total of 10,405 ankyrin-G-IR AIS, 18,900 βIV spectrin-SD-IR AIS, and 6,315 gephyrin-IR AIS were counted in this study. The total number of labeled AIS counted per animal ranged from 22 to 412 for ankyrin-G-IR AIS, 72 to 471 for βIV spectrin-SD-IR AIS, and 6 to 245 for gephyrin-IR AIS. The sampling parameters resulted in mean (± SD) coefficients of error (CE) of .09 ± .02 for ankyrin-G-IR AIS, .07 ± .02 for βIV spectrin-SD-IR AIS, and .18 ± .04 for gephyrin-IR AIS. The higher CE for gephyrin-IR AIS reflects the very low numbers of gephyrin-IR AIS in some age groups, as well as the restricted laminar distribution, which resulted in greater variability in numbers of these profiles across counting frames.

Gephyrin-IR and ankyrin-G-IR AIS were quantified by E.M.L. and βIV spectrin-SD-IR AIS were quantified by S.D.S. The slides were coded so that the rater was blind to the subject number and age of each specimen. The intra-rater reliability of AIS counts was confirmed by intra-class correlation coefficients (ICC) of .991 (95% confidence interval [CI] = .949-.998) for ankyrin-G-IR AIS, .991 (95% CI = .954-.998) for βIV spectrin-SD-IR AIS, and .996 (95% CI = .976-.999) for gephyrin-IR AIS. The ICC for inter-rater reliability of AIS counts between D.A.C. and E.M.L. for ankyrin-G-IR and gephyrin-IR AIS were .932 (95% CI = .726-.983) and .975 (95% CI = .876-.995), respectively. The ICC for inter-rater reliability of AIS counts between D.A.C. and S.D.S. for βIV spectrin-SD-IR AIS was .985 (95% CI = .940-.996).

In order to determine the laminar distribution of gephyrin-IR and ankyrin-G-IR AIS in the same portion of area 46, a second analysis was performed using the Neurolucida program (MicroBrightfield, Inc., Colchester, VT). For each section, using a 40x PlanApo objective, the location of all labeled structures of interest were identified on a video monitor (final magnification = 960x) and plotted in a 450-μm-wide pia to white matter traverse at the midpoint of the dorsal bank of the principal sulcus. The labeled AIS were then separated into cortical layers based upon the percent of cortical depth, as determined from adjacent Nissl-stained sections.

To assess whether age differences in density were influenced by changes in length of the labeled structures, we measured the lengths of ankyrin-G-IR, βIV spectrin-SD-IR, and gephyrin-IR AIS in the three age groups (groups 1, 5 and 7) that showed the largest differences in density of labeled AIS. Using the Neurolucida program and a 100x oil-immersion objective, 25 AIS per subject in layers 2 and 5 of area 46, as identified from adjacent Nissl sections, were traced from a video monitor at a final magnification of 2400x.

Statistical analyses

For the regional density measures, analyses of variance (ANOVAs) were conducted with the cortical density of AIS as the dependent variable and age group as the main effect. In the laminar distribution analysis, an ANOVA was conducted for each cortical layer measured, with the mean percent of labeled AIS in that layer as the dependent variable and age group as the main effect. For the length measurements, an ANOVA was conducted for each cortical layer measured, with the length of labeled AIS in a layer as the dependent variable and age group as the main effect. For each ANOVA with a significant result, the Least Significant Difference post-hoc test was used to compare the differences between age groups, with $\alpha = .05$.

Photography

The photomicrographs presented in this study were generated using a Zeiss Axiocam camera. Photomontages were assembled and brightness and contrast were adjusted in Adobe Photoshop.

Results

Morphology of ankyrin-G-, βIV spectrin-SD-, and gephyrin-labeled structures

Ankyrin-G-IR AIS appeared as intensely labeled, vertically-oriented structures that were widest just below the unlabeled soma of pyramidal neurons and progressively tapered in diameter with increasing distance from the soma (Fig. 1A). Ankyrin-G-IR AIS in the youngest monkeys appeared to be much longer than those in the adult monkeys (Fig. 2C,D). A small number of ankyrin-G-labeled structures, most prominent in layer 1 (Fig. 2A), were quite thin and tortuous, and because they lacked the distinctive features of AIS, they were not quantified. Ankyrin-G immunoreactivity was also present in small punctate structures in the cortex (Fig. 1A) and most predominantly in the white matter. These punctate structures likely represent the presence of ankyrin-G at nodes of Ranvier in myelinated axons (Jenkins and Bennett, 2002;Zhou et al., 1998).

The appearance of βIV spectrin-SD-IR AIS was quite similar to that of ankyrin-G-IR AIS: intensely-labeled, vertically-oriented structures that tapered with increasing distance from the soma (Fig. 1B). βIV spectrin-SD-IR AIS appeared to be the longest in the youngest monkeys and to shorten with increasing age (Fig. 3C,D). βIV spectrin-SD immunoreactivity was also present in small punctate structures in the cortex (Fig. 1B) with a much greater density of punctate labeling in the white matter; these punctate profiles likely reflect the presence of βIV spectrin-SD at nodes of Ranvier (Berghs et al., 2000;Yang et al., 2007).

Gephyrin-IR AIS also were identified as thin, tapering, vertically-oriented structures located below the unlabeled cell bodies of pyramidal neurons (Fig. 1C; Fig. 4). In contrast to ankyrin-G and βIV spectrin-SD (Fig. 1A,B), gephyrin immunoreactivity in AIS appeared as aggregates of punctate labeling (Fig. 1C). In addition, isolated gephyrin-IR puncta were present in the cortical neuropil (Fig. 1C), presumably reflecting its association with $GABA_A$ receptors at locations other than the AIS, but not in the white matter. Gephyrin-IR AIS also appeared to be shorter than both ankyrin-G-IR and ßIV spectrin-SD-IR AIS, especially in the youngest animals (compare Figs. 2C, 3C and 4C).

Overall cortical densities of ankyrin-G- and gephyrin-IR AIS

Qualitative impressions of age-related differences in the relative density of ankyrin-G-IR AIS (Fig. 2) were confirmed by blinded quantitative analyses. As shown in Figure 5A, the density of ankyrin-G-IR AIS was greatest at birth and then progressively declined until about 4 years of age. ANOVA revealed a significant ($F_{6,26} = 10.28$, $P < .001$) effect of age

group on ankyrin-G-IR AIS density (Fig. 5B). Post hoc analyses (Fig. 5B) revealed a significant 67% decline in ankyrin-G-IR AIS density between the animals <1 month of age (age group 1) and those 3-4 years of age (age group 6).

The general developmental trajectory of βIV spectrin-SD immunoreactivity (Fig. 3) in area 46 was similar to that of ankyrin-G, although the slope of the early developmental decline in density appeared to be steeper for βIV spectrin-SD. The density of βIV spectrin-SD-IR AIS was greatest immediately after birth, and then declined until approximately 5 months postnatal when the labeled AIS reached a density that remained stable through adulthood (Fig. 5C). ANOVA revealed a significant ($F_{6,26} = 33.13$, $P < .001$) effect of age group on βIV spectrin-SD-IR AIS density (Fig. 5D); significant declines in βIV spectrin-SD-IR AIS density between the <1 month old (age group 1), 1-3 month old (age group 2), and 5-7 month old (age group 3) animals was confirmed by post hoc analyses (Fig. 5D). The density of βIV spectrin-SD -IR AIS was 40% lower in age group 3 than in age group 1.

The relative density of gephyrin-IR AIS (Fig. 4) also decreased substantially during postnatal development, but with a different trajectory than either ankyrin-G or βIV spectrin-SD. Although variable across animals, gephyrin-IR AIS density did not appear to change through the first year or two postnatal, but then sharply declined through adolescence and into adulthood (Fig. 5E). ANOVA showed a significant ($F_{6,26} = 12.58$, $P < .001$) effect of age group on gephyrin-IR AIS density, and post hoc analyses revealed significant declines in gephyrin-IR AIS density at 2 years of age and after 4 years of age (Fig. 5F). Relative to the first 7 months of life (age groups 1-3), the densities of gephyrin-IR AIS were approximately 40% lower in adolescent monkeys (age groups 5 and 6) and approximately 80% lower in adult monkeys more than 5 years old (age group 7).

Laminar distributions of ankyrin-G-, βIV spectrin-SD-, and gephyrin-IR AIS

Ankyrin-G-IR structures meeting criteria for labeled AIS were present in layers 2 through 6 in all animals (Fig. 6A). Quantitative analyses showed that the percentage of AIS did not differ across postnatal development in layer 3 ($F_{6,26} = 2.1$, $P = .086$), layer 4 ($F_{6,26} = 1.125$, $P = .376$), or layers 5-6 ($F_{6,26} = 0.6$, $P = .763$); in contrast, the percentage of ankyrin-G-IR AIS in layer 2 did significantly differ ($F_{6,26} = 4.9$, $P = .002$) as a function of age. Post-hoc analysis revealed that the percentage of labeled AIS in layer 2 was slightly but significantly ($P < .001$ - $.043$) greater in age group 6 than in each of the younger age groups, but did not differ from age group 7. βIV spectrin-SD-IR AIS were also present in layers 2 through 6 in all animals (Fig. 6B), with a laminar distribution similar to that found for ankyrin-G-IR AIS (Fig. 6A) and without evidence of a shift in laminar distribution with age.

In animals less than 1 month of age, gephyrin-IR AIS were present primarily in layers deep 3 and 4, with a lower density in layers 5-6 (Fig. 6C). From 1 month to 2 years of age, the percentage of labeled AIS in these layers remained high, and the number of labeled AIS progressively increased in layer 2. After 2 years of age, the density of gephyrin-IR AIS in the middle and deep cortical layers substantially decreased, such that in adolescent (3-4 years of age) and adult (>5 years of age) animals, labeled AIS formed bands in layers 2 and 4, with a lower density in layer 3. Quantitative analyses revealed that the mean percentage of AIS did not significantly differ with age in layers 2 ($F_{6,26} = 1.2$, $P = .323$) or 3 ($F_{6,26} = 0.6$, $P = .730$). However, the mean percentage of gephyrin-IR AIS significantly increased during postnatal development in layer 4 ($F_{6,26} = 2.9$, $P = .025$) and declined in layers 5-6 ($F_{6,26} = 5.4$, $P = .001$).

Length of AIS

The lengths of AIS immunoreactive for ankyrin-G, βIV spectrin-SD, or gephyrin measured in cortical layers 2 and 5 (Fig. 7) revealed significant differences across age groups 1 (<1 month of age), 5 (2-3 years of age), and 7 (>5 years of age). The length of ankyrin-G-IR AIS significantly differed with age in both layer 2 ($F_{2,14}$=31.1, $P < .001$) and layer 5 ($F_{2,14}$ = 20.8, $P < .001$). Post-hoc analyses revealed that in layer 2, labeled AIS length significantly decreased from age group 1 to age groups 5 and 7 (Fig. 7A), whereas in layer 5 the length of labeled AIS progressively decreased with age across all three age groups (Fig. 7B). The length of βIV spectrin-SD-IR AIS also significantly differed with age in both layer 2 ($F_{2,18}$ = 20.9, $P < .001$) and layer 5 ($F_{2,18}$ = 39.0, $P <.001$), and post-hoc analyses revealed that the length significantly decreased with age across all three age groups in both layers (Fig. 7C, D). In contrast, the length of gephyrin-IR AIS (Fig. 8E, F) did not differ as a function of age in either layer 2 ($F_{2,14}$ = 2.3, P =.141) or layer 5 ($F_{2,14}$ = 1.2, P =.341).

Discussion

These findings demonstrate that pyramidal neuron AIS immunoreactive for ankyrin-G, βIV spectrin-SD or gephyrin in the monkey PFC undergo substantial changes in relative density, laminar distribution and/or length during postnatal development. Furthermore, differences among the developmental trajectories of these and other markers of chandelier cell inputs to pyramidal neurons (Anderson et al., 1995; Cruz et al., 2003) suggest that the maturation of the molecular mechanisms that influence GABA neurotransmission at the AIS of pyramidal neurons is a complex and protracted process in primates (Fig. 8).

In the monkey PFC, the density of GABA synapses increases markedly during the last trimester of gestation and first 3 months of postnatal life, achieving a stable level that is maintained through adolescence and into adulthood (Bourgeois et al., 1994). In contrast, markers of the functional properties of inhibitory synapses, as well as electrophysiological features, substantially change during adolescence in monkey PFC (Cruz et al., 2003; Erickson and Lewis, 2002; Nguyen et al., 2006). These findings are supported by the observation that the expression of mRNA for GABA synthesizing enzymes also change during adolescence in human PFC (Huang et al., 2007). Together, these observations suggest that the developmental changes observed in the densities of labeled AIS reflect age-related differences in the molecular architecture of this structure.

Excitatory synapses also substantially increase in density from the third trimester of gestation through the third month postnatal and retain this elevated level until ~1.5 years of age; density then declines markedly during adolescence before stable adult levels are achieved (Bourgeois et al., 1994; Anderson et al., 1995). Interestingly, excitatory synapses in monkey PFC appear to become functionally mature before the adolescence-associated decline in number (Gonzalez-Burgos et al., 2008). Thus, inhibitory and excitatory synapses exhibit different patterns of structural and functional maturation in the primate PFC, suggesting the presence of age-related differences in how inhibitory-excitatory balance is maintained. These developmental changes are particularly important at the AIS of pyramidal neurons where GABA inputs from chandelier neurons can exert potent inhibitory or excitatory effects (Klausberger et al., 2003; Szabadics et al., 2006). The findings of the present study provide insight into the role of several post-synaptic proteins in the maturation of these GABA inputs.

Developmental trajectories of AIS markers

The greatest densities of ankyrin-G-IR, βIV spectrin-SD-IR, and gephyrin-IR AIS were present immediately after birth (Fig. 8). Ankyrin-G localizes and retains the cell adhesion

molecule, neurofascin 186, to the AIS of projection neurons (Ango et al., 2004;Boiko et al., 2007). Through its interaction with ankyrin-G, neurofascin 186 is responsible for the recruitment of GABA synapses to the AIS of cerebellar purkinje neurons (Ango et al., 2004). If this same mechanism is operative in cortical pyramidal neurons, then the high density of AIS with detectable levels of ankyrin-G immunoreactivity in the first three postnatal months may reflect the recruitment to this location of a portion of the large number of GABA synapses that are formed in the PFC during this developmental epoch (Bourgeois et al., 1994). Binding to ankyrin G is also essential for the localization of many other membrane proteins to the AIS (Susuki and Rasband, 2008), including the voltage-gated Na^+ channels that are required for action potential generation (Zhou et al., 1998). Thus, the high levels of ankyrin G immunoreactivity may also indicate an increased capacity of pyramidal neurons for repetitive firing that parallels their increase in excitatory inputs during early postnatal development (Bourgeois et al., 1994;Anderson et al., 1995).

The parallel relative densities of ankyrin-G-IR and βIV spectrin-SD-IR AIS likely reflect that ankyrin-G is required for the recruitment of βIV spectrin to AIS (Yang et al., 2007). Although βIV spectrin is not essential for the formation of the AIS, it does appear necessary for maintenance of membrane structure and molecular organization (Lacas-Gervais et al., 2004), and thus the stability (Yang et al., 2007), of AIS. Given the general role of spectrins in maintaining membrane integrity and elasticity (Susuki and Rasband, 2008), high levels of βIV spectrin during early postnatal development might insure the stability of AIS structure while prefrontal cortical thickness is increasing (Rabinowicz, 1974; Giedd et al., 1999).

The densities of both ankyrin-G- and βIV spectrin-SD-IR AIS significantly declined between 3 and 5 months of age, but then remained stable during the remainder of development, including adolescence (Fig. 5B,D). The parallel decline in these markers immediately follows the establishment of adult densities of symmetric synapses in monkey PFC (Bourgeois et al., 1994). These comparisons suggest that once GABA synapses are recruited to the AIS via the interaction of ankyrin-G, neurofascin 186, and βIV spectrin-SD (Ango et al., 2004; Davis and Bennett, 1984; Bennett and Baines, 2001), reduced levels of ankyrin-G and βIV spectrin-SD (reflected in a lower number of AIS with detectable levels of immunoreactivity) are able to sustain a steady-state number of GABA synapses.

The high density of gephyrin-IR AIS during early postnatal development is accompanied by a high density of AIS immunoreactive for $GABA_A$ receptors containing the α_2 subunit (Cruz et al., 2003), consistent with the role of gephyrin in clustering this type of $GABA_A$ receptor (Tretter et al., 2008). In contrast, during this same developmental epoch, the densities of parvalbumin (PV)-IR and GABA membrane transporter (GAT1)-IR chandelier cell axon cartridges (Cruz et al., 2003) are very low (Fig. 8). At presynaptic terminals, PV is thought to reduce Ca^{2+}-dependent GABA release (Vreugdenhil et al., 2003) and the amount of GAT1 is inversely correlated with the availability of GABA at the synapse (Mager et al., 1993; Isaacson et al., 1993). Together, these findings suggest that both the release of GABA from chandelier axon cartridges, and its persistence in the extracellular space at AIS, is very high during early postnatal development. In concert with the high density of both gephyrin-IR and $GABA_A$ β_2-IR AIS, these findings suggest that both pre- and post-synaptic factors are shifted to maximize GABA neurotransmission at pyramidal cell AIS during the first months of postnatal development. This convergence of factors likely promotes the formation and stabilization of synapses at this site as suggested by the findings that the expression of the 67 kD form of glutamic acid decarboxylase, the principal determinant of GABA levels, is essential for the development of GABA axons and synapses, at least in cortical basket neurons (Chattopadhyaya et al., 2007). Furthermore, since gephyrin and $GABA_A$ receptors containing the α_2 subunit preferentially form clusters opposite GABA terminals, high levels

of gephyrin may enhance the stability of these $GABA_A$ receptor clusters by limiting their diffusion and by confining them to the synapse (Studler et al., 2005; Jacob et al., 2005).

The density of gephyrin-IR AIS remained high through the first two years postnatal, but then markedly declined from approximately 2 to 4 years of age (Fig. 8), the period of adolescence in macaque monkeys. This trajectory strikingly parallels those of both pre- (PV and GAT1) and post- ($GABA_A$ receptor α2 subunit) synaptic markers of GABA inputs to the AIS (Cruz et al., 2003). Together, these findings suggest a marked adolescence-related shift in the chandelier cell regulation of pyramidal neuron output. Recent molecular and electrophysiological findings indicate that the developmental shift in $GABA_A$ receptors from a predominance of α2 to α1 subunits (Fritschy et al., 1994) continues through adolescence in monkey PFC (Nguyen et al., 2006). Since gephyrin preferentially clusters with $GABA_A$ receptors containing α2, but not α1, subunits (Tretter et al., 2008), the decline in gephyrin immunoreactivity may reflect a substitution of α1 for α2 subunits at the AIS during adolescence. Since α1-containing GABA receptors are associated with a much faster decay of inhibitory postsynaptic currents than those containing α2 subunits (Farrant and Nusser, 2005), these findings (in concert with an increased availability of extracellular GABA due to reductions in presynaptic PV and GAT1), suggest that both the speed and strength of GABA neurotransmission at the AIS markedly increase during adolescence. Given the importance of prefrontal GABA neurotransmission in working memory (Rao et al., 1999;Rao et al., 2000;Sawaguchi et al., 1989), these changes might contribute to the improved working memory performance that occurs during adolescence in primates (Luna et al., 2004;Crone et al., 2006;Diamond, 2002).

Ankyrin-G-IR and gephyrin-IR AIS exhibited shifts in their laminar distributions across postnatal development, indicating that subpopulations of pyramidal neuron AIS might be differentially regulated by GABA inputs at any given age. For example, the increased percentage of ankyrin-G-IR AIS in layer 2 during adolescence suggests that a subpopulation of corticocortically projecting pyramidal neurons experience adolescence-related refinements in the number of GABA inputs to the AIS. In addition, the laminar distribution of gephyrin-IR AIS also changed substantially across development (Fig. 6). These findings suggest that pyramidal neurons with different projection targets (Jones, 1984) also differ in their need for GABA regulation at the AIS across development, an interpretation supported by the observation of cell type and laminar differences in the number of symmetric, presumably GABA, synapses at pyramidal neuron AIS in adult primate cortex (Farinas and DeFelipe, 1991). Consistent with this interpretation, other studies suggest that there may also be heterogeneity in the chandelier subclass of GABAergic neurons. For example, the detectability of chandelier neuron axon terminals (cartridges) with different biochemical markers differs both across (Lewis et al., 1989;Akil and Lewis, 1992;Condé et al., 1996) and within cortical regions (Lewis and Lund, 1990).

During the first postnatal month, the mean lengths of ankyrin-G-IR and βIV spectrin-SD-IR AIS were approximately twice that of gephyrin-IR AIS (Fig. 7), a difference that disappeared with age. This marked difference in length during early development may reflect incomplete myelination of the PFC as both ankyrin-G and βIV spectrin-SD are localized to the myelin-free AIS and nodes of Ranvier (Hedstrom and Rasband, 2006). Thus, as myelination of projection neuron axons progresses, the distribution of proteins that define the AIS, and its presynaptic inputs, becomes more restricted. Consistent with this interpretation, the length of markers of pre-synaptic chandelier neuron axon cartridges, such as GAT1 and PV immunoreactivity, also declines with age (Cruz et al., 2003). The developmental changes in length of ankyrin-G immoreactivity might also reflect an activity-dependent plasticity of AIS structure that, by shifting the location of voltage-gated Na^+

channels, adjusts the proximity of the site of action potential generation to the cell body and hence the firing efficacy of the neuron (Kuba et al., 2006).

In contrast to the measures of ankyrin-G-IR and βIV spectrin-SD-IR AIS, the length of gephyrin immunoreactivity within AIS did not change with age. Gephyrin facilitates the localization of $GABA_A$ receptors containing the α_2 subunit to the AIS of pyramidal neurons by restricting the lateral mobility of GABA receptor clusters to the synapse (Jacob et al., 2005); thus, the location of clusters of $GABA_A$ receptors in the AIS appears to be constant across development, an interpretation supported by the absence of a change with age in the length of AIS immunoreactive for $GABA_A$ receptor α_2 subunits (Cruz et al., 2003).

Methodologic considerations

The quantification of labeled AIS density in this study utilized a systematic and random approach in order to reduce sampling bias. However, the total number of IR structures could not be estimated due to the unavailability of all of area 46 for study; thus, because area 46 was not uniformly sampled, these results may not apply to the entire region. On the other hand, the different postnatal developmental trajectories of ankyrin-G-, βIV spectrin-SD-, and gephyrin-IR AIS densities suggest that the results are not due to systematic confounds in sampling.

The density estimates of labeled AIS may have been affected by changes in cortical volume that occur during postnatal development (Giedd et al., 1999; Sowell et al., 2001). Although cortical thickness did not significantly differ across age groups ($F_{(6,33)} = .688$, $p = .661$), comparisons between age groups 1 and 4 (birth to pre-adolescence) and age groups 4 and 7 (preadolescence to adult), revealed a 3.6% increase and a 18.5% decrease, respectively, in cortical thickness. The increase in cortical thickness across age groups 1-4 appears to be too small to account for the decreases observed in ankyrin-G-IR and ßIV-spectrin-IR AIS density in these animals. Consistent with this interpretation, the density of gephyrin-IR AIS did not decrease during this developmental epoch. The apparent decrease in cortical thickness across age groups 4-7 would actually lead to an underestimation of the degree of decline in gephyrin-IR AIS density. Importantly, across all age groups, cortical thickness was not significantly associated with AIS density for ankyrin-G, ßIV-spectrin, or gephyrin ($r = -.130$, $p = .470$; $r = -.130$, $p = .470$; and $r = .006$, $p = .974$, respectively). Thus, although we cannot definitively exclude an effect of changes in cortical volume on our density measures, these findings, and the differences in developmental trajectories of AIS measures shown in summary Figure 8, converge on the interpretation that the observed changes in density of labeled AIS reflect shifts in the amounts of the targeted proteins (and thus the detectability of immunoreactive AIS) rather than in the actual density of AIS.

Because the length of a labeled profile can influence the likelihood that it will be present and counted in a given section, we assessed the mean length of immunoreactive AIS in age groups 1 (<1 month), 5 (2-3 years), and 7 (>5 years), the age groups that showed the greatest differences in the mean densities of labeled AIS (Fig. 5). The mean length of ankyrin-G-IR and βIV spectrin-SD-IR AIS decreased significantly across all three age groups examined (Fig. 7A-D), whereas their densities remained stable between age groups 5 and 7 (Fig. 5B, D). This dissociation suggests that the differences in length did not likely affect density measures, probably because any such effects were minimized by the strategy of counting AIS only in areas of the cortex cut perpendicular to the pial surface (and thus parallel to the long axis of AIS) where their presence and identification would be unlikely to be affected by their length. Consistent with this interpretation, the marked differences in the relative densities of gephyrin-IR AIS across these age groups (Fig. 5F) were not associated with any differences in mean length of labeled AIS (Fig. 7 E, F).

This study included both male and female animals; however, sex does not appear to have had an influence on the findings. For example, analyses of the mean densities of AIS immunoreactive for ankyrin-G, βIV spectrin-SD, or gephyrin in age groups 1 (<1 month), 4 (1-2 years), and 7 (>5 years), that contain both male and female animals, showed no within-group differences by sex (all $P > .629$, unpaired *t* tests). Additionally, across sections labeled for ankyrin-G, βIV spectrin-SD or gephyrin, the coefficient of variance (CV) in the mixed sex age groups 1, 4, and 7 (CV range 0.08 to 0.51) did not differ from CVs of the same sex age groups (CV range 0.07 to 0.49; $P > 0.552$, unpaired *t* test).

Conclusions

The results of these studies indicate that molecular determinants of the structural features that define GABA inputs to pyramidal neuron AIS in monkey PFC undergo distinct developmental trajectories with different types of changes occurring during the perinatal period and adolescence. In concert with previous data, these findings reveal a two-phase developmental process of GABAergic synaptic stability and GABA neurotransmission at chandelier cell inputs to pyramidal neurons that likely contributes to the protracted maturation of behaviors mediated by primate PFC circuitry.

Acknowledgments

Supported by NIH grant MH051234 from the National Institute of Mental Health. The content is solely the responsibility of the authors and does not necessarily represent the official views of the National Institute of Mental Health or the National Institutes of Health.

Literature Cited

Akil M, Lewis DA. Differential distribution of parvalbumin-immunoreactive pericellular clusters of terminal boutons in developing and adult monkey neocortex. Exp Neurol. 1992; 115:239–249. [PubMed: 1735469]

Anderson SA, Classey JD, Condé F, Lund JS, Lewis DA. Synchronous development of pyramidal neuron dendritic spines and parvalbumin-immunoreactive chandelier neuron axon terminals in layer III of monkey prefrontal cortex. Neuroscience. 1995; 67:7–22. [PubMed: 7477911]

Ango F, Di Cristo G, Higashiyama H, Bennett V, Wu P, Huang ZJ. Ankyrin-based subcellular gradient of neurofascin, an immunoglobulin family protein, directs GABAergic innervation at purkinje axon initial segment. Cell. 2004; 119:257–272. [PubMed: 15479642]

Ascoli GA, Alonso-Nanclares L, Anderson SA, Barrionuevo G, Benavides-Piccione R, Burkhalter A, Buzsaki G, Cauli B, DeFelipe J, Fairen A, Feldmeyer D, Fishell G, Fregnac Y, Freund TF, Gardner D, Gardner EP, Goldberg JH, Helmstaedter M, Hestrin S, Karube F, Kisvarday ZF, Lambolez B, Lewis DA, Marin O, Markram H, Munoz A, Packer A, Petersen CC, Rockland KS, Rossier J, Rudy B, Somogyi P, Staiger JF, Tamas G, Thomson AM, Toledo-Rodriguez M, Wang Y, West DC, Yuste R. Petilla terminology: nomenclature of features of GABAergic interneurons of the cerebral cortex. Nat Rev Neurosci. 2008; 9:557–568. [PubMed: 18568015]

Bennett V, Baines AJ. Spectrin and ankyrin-based pathways: Metazoan inventions for integrating cells into tissues. Physiol Rev. 2001; 81:1353–1392. [PubMed: 11427698]

Berghs S, Aggujaro D, Dirkx R, Maksimova E, Stabach P, Hermel JM, Zhang JP, Philbrick W, Slepnev V, Ort T, Solimena M. beta IV spectrin, a new spectrin localized at axon initial segments and nodes of ranvier in the central and peripheral nervous system. J Cell Biol. 2000; 151:985–1001. [PubMed: 11086001]

Boiko T, Vakulenko M, Ewers H, Yap CC, Norden C, Winckler B. Ankyrin-dependent and -independent mechanisms orchestrate axonal compartmentalization of L1 family members neurofascin and L1/neuron-glia cell adhesion molecule. J Neurosci. 2007; 27:590–603. [PubMed: 17234591]

Bourgeois J-P, Goldman-Rakic PS, Rakic P. Synaptogenesis in the prefrontal cortex of rhesus monkeys. Cereb Cortex. 1994; 4:78–96. [PubMed: 8180493]

Burkarth N, Kriebel M, Kranz EU, Volkmer H. Neurofascin regulates the formation of gephyrin clusters and their subsequent translocation to the axon hillock of hippocampal neurons. Mol Cell Neurosci. 2007; 36:59–70. [PubMed: 17681789]

Chattopadhyaya B, Di Cristo G, Wu CZ, Knott G, Kuhlman S, Fu Y, Palmiter RD, Huang ZJ. GAD67-mediated GABA synthesis and signaling regulate inhibitory synaptic innervation in the visual cortex. Neuron. 2007; 54:889–903. [PubMed: 17582330]

Condé F, Lund JS, Lewis DA. The hierarchical development of monkey visual cortical regions as revealed by the maturation of parvalbumin-immunoreactive neurons. Dev Brain Res. 1996; 96:261–276. [PubMed: 8922688]

Crone EA, Wendelken C, Donohue S, van Leijenhorst L, Bunge SA. Neurocognitive development of the ability to manipulate information in working memory. Proc Natl Acad Sci U S A. 2006; 103:9315–9320. [PubMed: 16738055]

Cruz DA, Eggan SM, Lewis DA. Postnatal development of pre- and post-synaptic GABA markers at chandelier cell inputs to pyramidal neurons in monkey prefrontal cortex. J Comp Neurol. 2003; 465:385–400. [PubMed: 12966563]

Davis JQ, Bennett V. Brain ankyrin. A membrane-associated protein with binding sites for spectrin, tubulin, and the cytoplasmic domain of the erythrocyte anion channel. J Biol Chem. 1984; 259:13550–13559. [PubMed: 6092380]

Diamond, A. Normal development of prefrontal cortex from birth to young adulthood: Cognitive functions, anatomy and biochemistry. In: Stuss, DT.; Knight, RT., editors. Principles of Frontal Lobe Function. Oxford University Press; London: 2002. p. 466-503.

Erickson SL, Akil M, Levey AI, Lewis DA. Postnatal development of tyrosine hydroxylase- and dopamine transporter-immunoreactive axons in monkey rostral entorhinal cortex. Cereb Cortex. 1998; 8:415–427. [PubMed: 9722085]

Erickson SL, Lewis DA. Postnatal development of parvalbumin- and GABA transporter-immunoreactive axon terminals in monkey prefrontal cortex. J Comp Neurol. 2002; 448:186–202. [PubMed: 12012429]

Farinas I, DeFelipe J. Patterns of synaptic input on corticocortical and corticothalamic cells in the cat visual cortex. II. The axon initial segment. J Comp Neurol. 1991; 304:70–77. [PubMed: 2016413]

Farrant M, Nusser Z. Variations on an inhibitory theme: phasic and tonic activation of GABA(A) receptors. Nat Rev Neurosci. 2005; 6:215–229. [PubMed: 15738957]

Fritschy JM, Harvey RJ, Schwarz G. Gephyrin: where do we stand, where do we go? Trends Neurosci. 2008; 31:257–264. [PubMed: 18403029]

Fritschy J-M, Paysan J, Enna A, Mohler H. Switch in the expression of rat GABAA-receptor subtypes during postnatal development: An immunohistochemical study. J Neurosci. 1994; 14:5302–5324. [PubMed: 8083738]

Giedd JN, Blumenthal J, Jeffries NO, Castellanos FX, Liu H, Zijdenbos A, Paus T, Evans AC, Rapoport JL. Brain development during childhood and adolescence: a longitudinal MRI study. Nat Neurosci. 1999; 2:861–863. [PubMed: 10491603]

Gonzalez-Burgos G, Kroener S, Zaitsev AV, Povysheva NV, Krimer LS, Barrionuevo G, Lewis DA. Functional maturation of excitatory synapses in layer 3 pyramidal neurons during postnatal development of the primate prefrontal cortex. Cereb Cortex. 2008; 18:626–637. [PubMed: 17591597]

Hedstrom KL, Rasband MN. Intrinsic and extrinsic determinants of ion channel localization in neurons. J Neurochem. 2006; 98:1345–1352. [PubMed: 16787401]

Hsu S-M, Raine L, Fanger H. Use of avidin-biotin-peroxidase complex (ABC) in immunoperoxidase techniques: A comparison between ABC and unlabeled antibody (PAP) procedures. J Histochem Cytochem. 1981; 29:577–580. [PubMed: 6166661]

Huang HS, Matevossian A, Whittle C, Kim SY, Schumacher A, Baker SP, Akbarian S. Prefrontal dysfunction in schizophrenia involves mixed-lineage leukemia 1-regulated histone methylation at GABAergic gene promoters. J Neurosci. 2007; 27:11254–11262. [PubMed: 17942719]

Isaacson JS, Solis JM, Nicoll RA. Local and diffuse synaptic action of GABA in the hippocampus. Neuron. 1993; 10:165–175. [PubMed: 7679913]

Jacob TC, Bogdanov YD, Magnus C, Saliba RS, Kittler JT, Haydon PG, Moss SJ. Gephyrin regulates the cell surface dynamics of synaptic GABA(A) receptors. J Neurosci. 2005; 25:10469–10478. [PubMed: 16280585]

Jenkins SM, Bennett V. Ankyrin-G coordinates assembly of the spectrin-based membrane skeleton, voltage-gated sodium channels, and L1 CAMs at Purkinje neuron initial segments. J Cell Biol. 2001; 155:739–745. [PubMed: 11724816]

Jenkins SM, Bennett V. Developing nodes of Ranvier are defined by ankyrin-G clustering and are independent of paranodal axoglial adhesion. Proc Natl Acad Sci U S A. 2002; 99:2303–2308. [PubMed: 11842202]

Jenkins SM, Kizhatil K, Kramarcy NR, Sen A, Sealock R, Bennett V. FIGQY phosphorylation defines discrete populations of L1 cell adhesion molecules at sites of cell-cell contact and in migrating neurons. Journal of Cell Science. 2001; 114:3823–3835. [PubMed: 11719549]

Jiao Y, Sun Z, Lee T, Fusco FR, Kimble TD, Meade CA, Cuthbertson S, Reiner A. A simple and sensitive antigen retrieval method for free-floating and slide-mounted tissue sections. J Neurosci Meth. 1999; 93:149–162.

Jones, EG. Laminar distribution of cortical efferent cells. In: Peters, A.; Jones, EG., editors. Cerebral Cortex. Vol. Vol. 1. Plenum Press; New York: 1984. p. 521-553.

Khirug S, Yamada J, Afzalov R, Voipio J, Khiroug L, Kaila K. GABAergic depolarization of the axon initial segment in cortical principal neurons is caused by the Na-K-2Cl cotransporter NKCC1. J Neurosci. 2008; 28:4635–4639. [PubMed: 18448640]

Klausberger T, Magill PJ, Marton LF, Roberts JDB, Cobden PM, Buzsaki G, Somogyi P. Brain-state- and cell-type specific firing of hippocampal interneurons in vivo. Nature. 2003; 421:844–848. [PubMed: 12594513]

Kordeli E, Lambert S, Bennett V. AnkyrinG. A new ankyrin gene with neural-specific isoforms localized at the axonal initial segment and node of Ranvier. J Biol Chem. 1995; 270:2352–2359. [PubMed: 7836469]

Kuba H, Ishii TM, Ohmori H. Axonal site of spike initiation enhances auditory coincidence detection. Nature. 2006; 444:1069–1072. [PubMed: 17136099]

Lacas-Gervais S, Guo J, Strenzke N, Scarfone E, Kolpe M, Jahkel M, De Camilli P, Moser T, Rasband MN, Solimena M. BetaIVSigma1 spectrin stabilizes the nodes of Ranvier and axon initial segments. J Cell Biol. 2004; 166:983–990. [PubMed: 15381686]

Levi S, Logan SM, Tovar KR, Craig AM. Gephyrin is critical for glycine receptor clustering but not for the formation of functional GABAergic synapses in hippocampal neurons. J Neurosci. 2004; 24:207–217. [PubMed: 14715953]

Lewis DA, Campbell MJ, Morrison JH. An immunohistochemical characterization of somatostatin-28 and somatostatin-28 (1-12) in monkey prefrontal cortex. J Comp Neurol. 1986; 248:1–18. [PubMed: 2873154]

Lewis DA, Foote SL, Cha CI. Corticotropin releasing factor immunoreactivity in monkey neocortex: An immunohistochemical analysis. J Comp Neurol. 1989; 290:599–613. [PubMed: 2613945]

Lewis DA, Lund JS. Heterogeneity of chandelier neurons in monkey neocortex: Corticotropin-releasing factor and parvalbumin immunoreactive populations. J Comp Neurol. 1990; 293:599–615. [PubMed: 2329196]

Loup F, Weinmann O, Yonekawa Y, Aguzzi A, Wieser H-G, Fritschy J-M. A highly sensitive immunofluorescence procedure for analyzing the subcellular distribution of $GABA_A$ receptor subunits in the human brain. J Histochem Cytochem. 1998; 46:1129–1139. [PubMed: 9742069]

Luna B, Garver KE, Urban TA, Lazar NA, Sweeney JA. Maturation of cognitive processes from late childhood to adulthood. Child Devel. 2004; 75:1357–1372. [PubMed: 15369519]

Lund JS, Lewis DA. Local circuit neurons of developing and mature macaque prefrontal cortex: Golgi and immunocytochemical characteristics. J Comp Neurol. 1993; 328:282–312. [PubMed: 7678612]

Mager S, Naeve J, Quick M, Labarca C, Davidson N, Lester HA. Steady states, charge movements, and rates for a cloned GABA transporter expressed in xenopus oocytes. Neuron. 1993; 10:177–188. [PubMed: 7679914]

Markram H, Toledo-Rodriguez M, Wang Y, Gupta A, Silberberg G, Wu C. Interneurons of the neocortical inhibitory system. Nat Rev Neurosci. 2004; 5:793–807. [PubMed: 15378039]

McBain CJ, Fisahn A. Interneurons unbound. Nat Rev Neurosci. 2001; 2:11–23. [PubMed: 11253355]

Nguyen QL, Hashimoto T, Lewis DA. Postnatal development of $GABA_A$ receptor á1 and á2 subunit mRNA expression in the monkey dorsolateral prefrontal cortex. Society for Neuroscience. 2006 Abstract . 2006.

Oeth KM, Lewis DA. Postnatal development of the cholecystokinin innervation of monkey prefrontal cortex. J Comp Neurol. 1993; 336:400–418. [PubMed: 8263229]

Pierri JN, Chaudry AS, Woo T-U, Lewis DA. Alterations in chandelier neuron axon terminals in the prefrontal cortex of schizophrenic subjects. Am J Psychiatry. 1999; 156:1709–1719. [PubMed: 10553733]

Pucak ML, Levitt JB, Lund JS, Lewis DA. Patterns of intrinsic and associational circuitry in monkey prefrontal cortex. J Comp Neurol. 1996; 376:614–630. [PubMed: 8978474]

Rabinowicz T. Some aspects of the maturation of the human cerebral cortex. Mod Probl Paediat. 1974; 13:44–56.

Rao SG, Williams GV, Goldman-Rakic PS. Isodirectional tuning of adjacent interneurons and pyramidal cells during working memory: Evidence for microcolumnar organization in PFC. J Neurophysiol. 1999; 81:1903–1916. [PubMed: 10200225]

Rao SG, Williams GV, Goldman-Rakic PS. Destruction and creation of spatial tuning by disinhibition: $GABA_A$ blockade of prefrontal cortical neurons engaged by working memory. J Neurosci. 2000; 20:485–494. [PubMed: 10627624]

Sawaguchi T, Matsumura M, Kubota K. Delayed response deficits produced by local injection of bicuculline into the dorsolateral prefrontal cortex in Japanese macaque monkeys. Exp Brain Res. 1989; 75:457–469. [PubMed: 2744104]

Somogyi P. A specific axo-axonal interneuron in the visual cortex of the rat. Brain Res. 1977; 136:345–350. [PubMed: 922488]

Somogyi P, Freund TF, Cowey A. The axo-axonic interneuron in the cerebral cortex of the rat, cat and monkey. Neuroscience. 1982; 7:2577–2607. [PubMed: 7155343]

Sowell ER, Thompson PM, Tessner KD, Toga AW. Mapping continued brain growth and gray matter density reduction in dorsal frontal cortex: Inverse relationships during postadolescent brain maturation. J Neurosci. 2001; 21:8819–8829. [PubMed: 11698594]

Studler B, Sidler C, Fritschy JM. Differential regulation of GABA(A) receptor and gephyrin postsynaptic clustering in immature hippocampal neuronal cultures. J Comp Neurol. 2005; 484:344–355. [PubMed: 15739236]

Susuki K, Rasband MN. Spectrin and ankyrin-based cytoskeletons at polarized domains in myelinated axons. Exp Biol Med (Maywood). 2008; 233:394–400. [PubMed: 18367627]

Szabadics J, Varga C, Molnar G, Olah S, Barzo P, Tamas G. Excitatory effect of GABAergic axo-axonic cells in cortical microcircuits. Science. 2006; 311:233–235. [PubMed: 16410524]

Tretter V, Jacob TC, Mukherjee J, Fritschy JM, Pangalos MN, Moss SJ. The clustering of GABA(A) receptor subtypes at inhibitory synapses is facilitated via the direct binding of receptor alpha 2 Subunits to gephyrin. J Neurosci. 2008; 28:1356–1365. [PubMed: 18256255]

Vreugdenhil M, Jefferys JG, Celio MR, Schwaller B. Parvalbumin-deficiency facilitates repetitive IPSCs and gamma oscillations in the hippocampus. J Neurophysiol. 2003; 89:1414–1422. [PubMed: 12626620]

Walker AE. A cytoarchitectural study of the prefrontal area of the macaque monkey. J Comp Neurol. 1940; 73:59–86.

Yang Y, Lacas-Gervais S, Morest DK, Solimena M, Rasband MN. BetaIV spectrins are essential for membrane stability and the molecular organization of nodes of Ranvier. J Neurosci. 2004; 24:7230–7240. [PubMed: 15317849]

Yang Y, Ogawa Y, Hedstrom KL, Rasband MN. beta IV spectrin is recruited to axon initial segments and nodes of Ranvier by ankyrinG. J Cell Biol. 2007; 176:509–519. [PubMed: 17283186]

Yu W, Jiang M, Miralles CP, Li RW, Chen G, de Blas AL. Gephyrin clustering is required for the stability of GABAergic synapses. Mol Cell Neurosci. 2007; 36:484–500. [PubMed: 17916433]

Zhou DX, Lambert S, Malen PL, Carpenter S, Boland LM, Bennett V. Ankyrin(G) is required for clustering of voltage-gated Na channels at axon initial segments and for normal action potential firing. J Cell Biol. 1998; 143:1295–1304. [PubMed: 9832557]

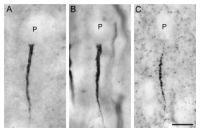

Figure 1.
Brightfield photomicrographs of pyramidal neuron AIS immunoreactive for ankyrin-G (A), ßIV spectrin-SD (B), and gephyrin (C) in area 46 of monkey prefrontal cortex. Punctate labeling in panel C likely represents gephyrin clusters at other GABA synapses. Scale bar = 5 μm in A (applies to A, B, C).

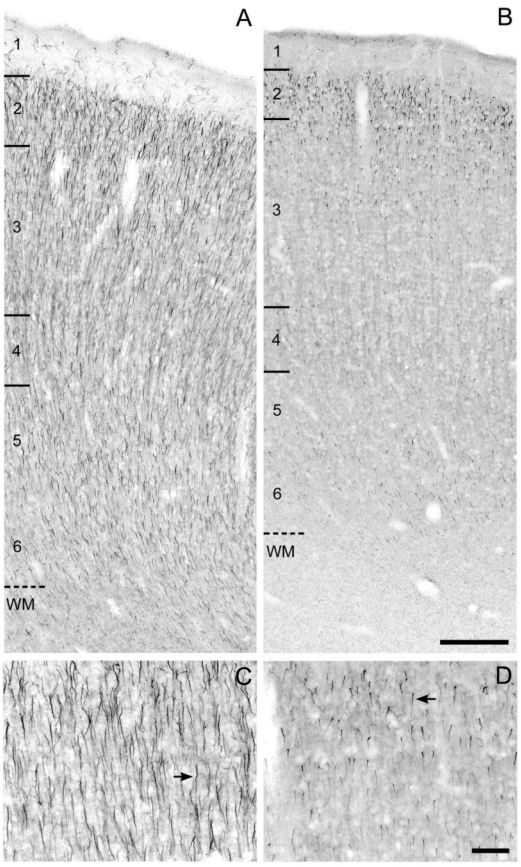

Figure 2.

Brightfield photomicrographs of ankyrin-G immunoreactivity in area 46 of monkeys 1 month (A,C) and 16.7 years (B,D) of age. The numbers and hash marks indicate laminar boundaries, and the dashed line indicates the layer 6-white matter (WM) border. The arrows indicate ankyrin-G immunoreactive AIS. The photomicrograph from Panel C is taken from superficial layer 3 in Panel A and the photomicrograph in Panel D is taken from layer 2 in Panel B. Scale bars = 200 μm in B (applies to A,B); 100 μm in D (applies to C,D).

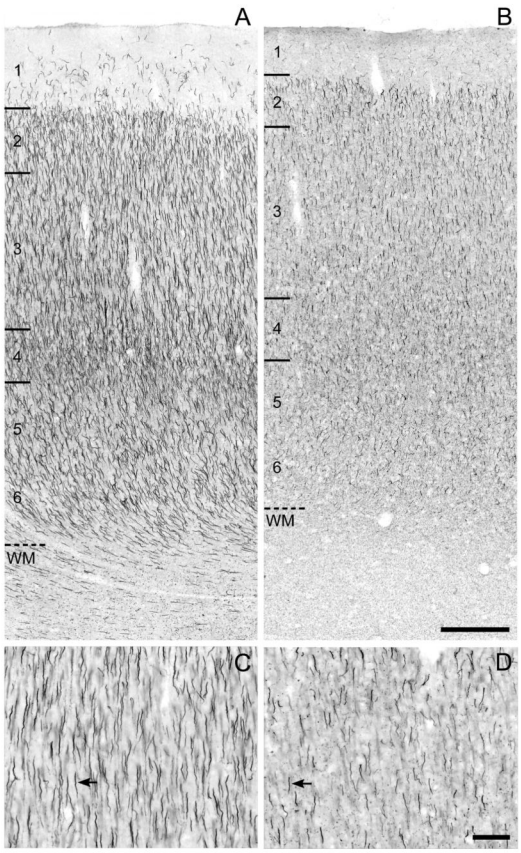

Figure 3.
Brightfield photomicrographs of ßIV spectrin-SD immunoreactivity in area 46 of monkeys 1 month (A,C) and 16.7 years (B,D) of age. The numbers and hash marks indicate laminar boundaries, and the dashed line indicates the layer 6-white matter (WM) border. The arrows indicate ßIV spectrin-SD immunoreactive AIS. The photomicrograph from Panel C is taken from superficial layer 3 in Panel A and the photomicrograph in Panel D is taken from layer 2 in Panel B. Scale bars = 200 μm in B (applies to A,B); 100 μm in D (applies to C,D).

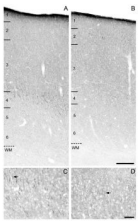

Figure 4.

Brightfield photomicrographs of gephyrin immunoreactivity in area 46 of monkeys 2.3 months (A,C) and 3.3 years (B,D) of age. The numbers and hash marks indicate laminar boundaries, and the dashed line indicates the layer 6-white matter (WM) border. The arrows indicate gephyrin immunoreactive AIS. The photomicrograph from Panel C is taken from layer 4 in Panel A and the photomicrograph in Panel D is taken from layer 2 in Panel B. Scale bars = 200 μm in B (applies to A,B); 100 μm in D (applies to C,D).

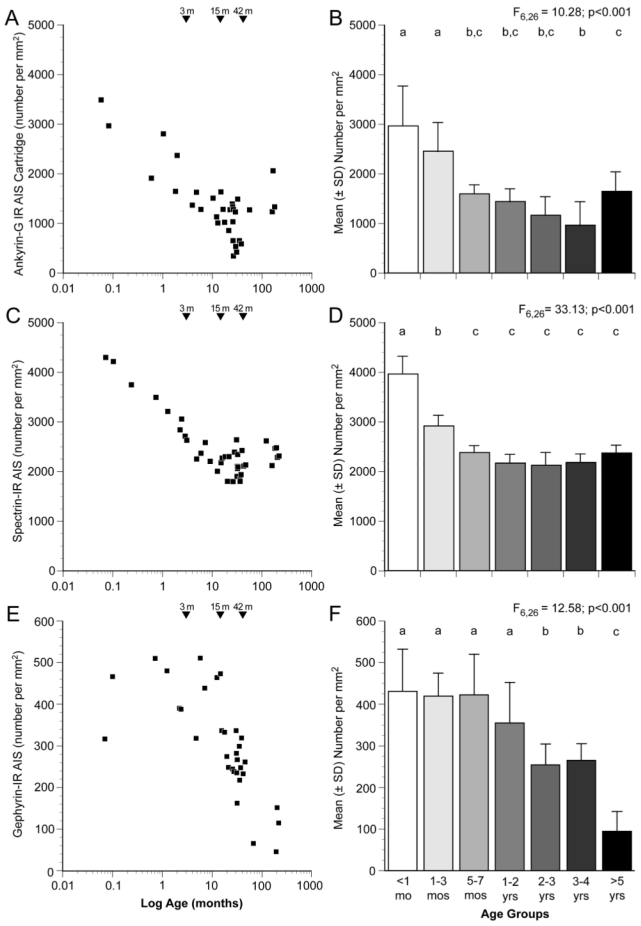

Figure 5.

Scatter plots of mean densities of ankyrin-G- (A), ßIV spectrin-SD- (C) and gephyrin-(E) immunoreactive AIS across all cortical layers for individual monkeys. Age in months after birth is plotted on a log scale. The bar graphs in the right column show the mean (± SD) densities of ankyrin-G (B), ßIV spectrin-SD (D) and gephyrin (F) immunoreactive AIS for each of the 7 age groups. Within each panel, age groups not sharing the same letter are significantly different at $P < 0.05$.

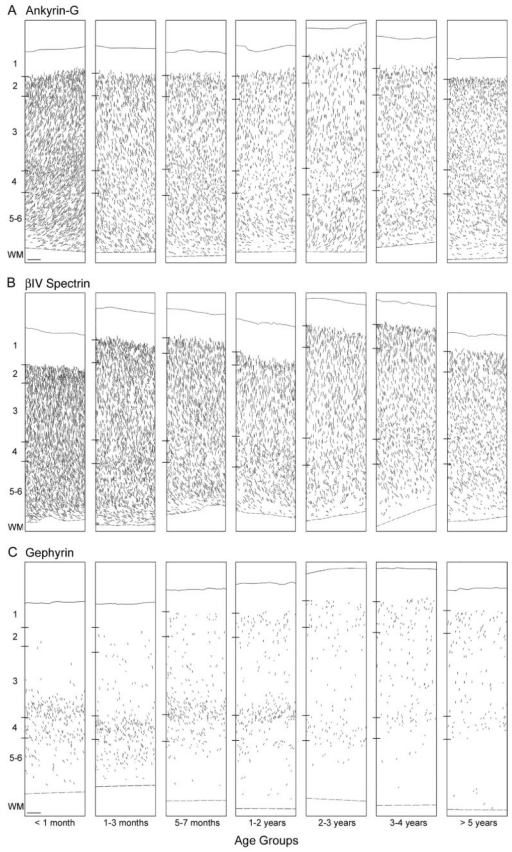

Figure 6.

Neurolucida drawings of a representative animal from each of the 7 age groups depicting the laminar distribution of ankyrin-G- (A), ßIV spectrin-SD- (B) and gephyrin- (C) immunoreactive AIS in area 46 of monkey prefrontal cortex. Each drawing represents a 450 μm-wide traverse from the pial surface (solid lines) to the layer 6-white matter border (dashed lines). Hash marks indicate the location of laminar boundaries; WM indicates white matter. Scale bar = 100 μm in C (applies to A,B,C).

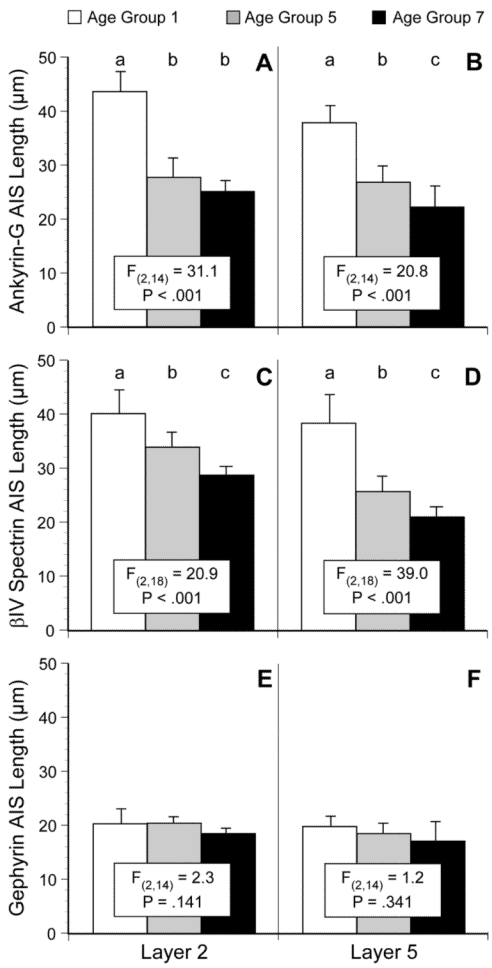

Figure 7.

Bar graphs showing the mean (± SD) length of AIS immunoreactive for ankyrin-G (A, B), ßIV spectrin-SD (C, D) or gephyrin (E, F) in layers 2 and 5 for age groups 1, 5, and 7 (see Table 1 for the age range of each group). Within each panel, age groups not sharing the same letter are significantly different at $P < 0.05$.

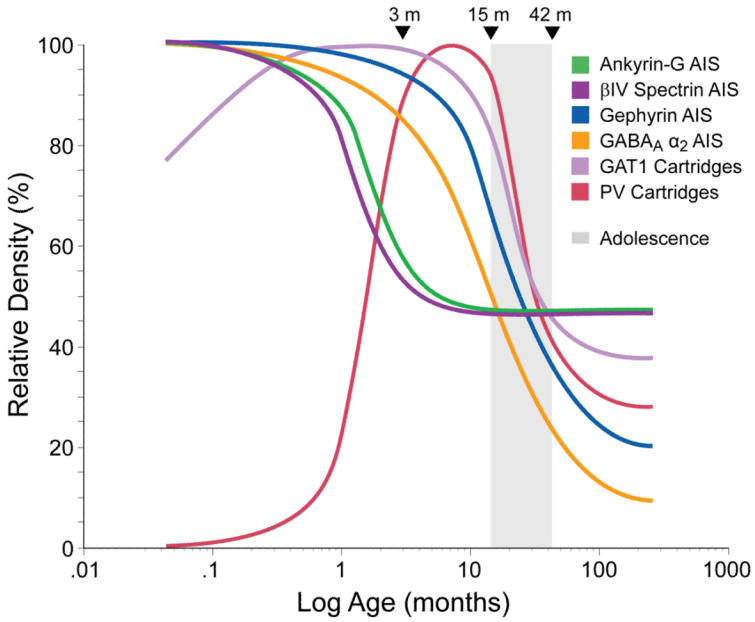

Figure 8.

Schematic summary of the trajectories of pyramidal neuron AIS and chandelier neuron axon cartridges labeled with difference markers across postnatal development in area 46 of monkey prefrontal cortex. Lines for each marker represent the percent maximal value achieved plotted against age in months after birth on a log scale. Arrowheads demarcate the indicated ages in months, and the shaded area indicates the approximate age range corresponding to adolescence in this species. GAT1 indicates GABA membrane transporter 1; PV indicates parvalbumin.

Table 1

Animals used in this study

					Processed for immunocytochemistry		
Age Group	**Subject**	**Age (m)**	**Weight (kg)**	**Sex**	**Ankyrin-G (n=33)**	**Gephyrin (n=33)**	**βIV Spectrin (n=40)**
1	142	0.07	0.3	M	•	•	•
	109	0.1	0.5	F	•	•	•
	272	0.23	0.6	F			•
	106	0.7	0.6	M	•	•	•
2	131	1.3	0.7	F	•	•	•
	130	2.3	0.8	F	•	•	•
	117	2.3	0.6	F	•	•	•
	271	2.8	1.1	F			•
	242	3	0.9	F			•
3	134	4.8	1.2	F	•	•	•
	155	5.8	1.2	F	•	•	•
	128	7.1	1.3	F	•	•	•
	274	8.9	2.3	F			•
4	133	12	1.9	F	•	•	•
	147	15	2.5	M	•	•	•
	146	16	2.5	M	•	•	•
	149	17	2.6	M	•	•	•
	135	18	2.8	F	•	•	•
	150	21	3.4	M	•	•	•
5	152	26	3.8	M	•	•	•
	154	27	4	M	•	•	•
	111	30	2.9	M	•	•	•
	158	31	4.5	M	•	•	•
	156	31	4.5	M	•	•	•
	153	31	4.6	M	•	•	•
	118	32	3.2	M	•	•	•
	163	32	3.7	M	•	•	•
	159	35	4.1	M	•	•	•

					Processed for immunocytochemistry		
Age Group	**Subject**	**Age (m)**	**Weight (kg)**	**Sex**	**Ankyrin-G (n=33)**	**Gephyrin (n=33)**	**βIV Spectrin (n=40)**
	160	36	5	M	•	•	•
6	167	37	5.9	M	•	•	•
	166	39	5.3	M	•	•	•
	170	42	6.2	M	•	•	•
	173	46	9.2	M	•	•	•
7	114	68	4.4	F	•	•	
	250	120	6.1	F			•
	217	156	11	F			•
	253	156	9.3	F			•
	254	180	10.4	F			•
	143	192	8.4	M	•	•	•
	112	200	7	F	•	•	•
	141	216	9	M	•	•	•